Journal of Hydraulic Structures
J. Hydraul. Struct., 2024;11(2):28-43
DOI: 10.22055/jhs.2024.47806.1319

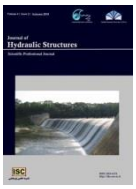

OPEN ACCESS

Simulation of Tsunami Waves Using Mike 3 Flow Model FM

Vahid Naderkhanloo [1]
Mohammad Hemmati [*1]
Hojjat Ahmadi [1]

Abstract

Tsunamis are a series of ocean waves with exceptionally long wavelengths and can be incredibly destructive when they reach coastal areas. These waves are typically triggered by underwater earthquakes, volcanic eruptions, or landslides. The immense force and energy of a tsunami wave can result in widespread devastation, flooding, and loss of life. It is crucial to comprehend the behavior of tsunami waves in order to develop effective early warning systems and strategies for managing such disasters. Numerical modeling has become a valuable tool for simulating the propagation of tsunamis and the processes of inundation. This research focuses on utilizing the Mike3 Flow Model FM for numerical modeling of tsunami waves. The model was tested using the results of solitary wave theory solutions and basic tsunami wave experiments conducted at the hydraulic laboratory of Changsha University in China. Statistical analysis of the numerical simulation results showed that the Mike3 Flow Model FM can provide accurate calculation of complex tsunami wave flows and deliver important results such as tsunami wave height, wave run-up length, flow volume, and temporal-spatial velocity profiles. Notably, the study observed an improvement in the accuracy of the numerical model as the ratio of wave height to water depth (H/h) decreased. Furthermore, it was confirmed that the accuracy of the numerical model in simulating wave velocity (RMSE $\leq$ 0.14) surpassed its performance in simulating wave surface elevation (RMSE $\leq$ 2.29), compared to experimental data.

Keywords: Tsunami Waves, Numerical Modeling, Mike3 Flow Model FM, Wave velocity, Wave surface elevation.

Received: 21 August 2024; Accepted: 14 September 2024

[*] Email: m.hemmati@urmia.ac.ir (**Corresponding Author**)
[1] Department of Water Engineering, Urmia University, Urmia, Iran.

1. Introduction

One way to reduce the damage caused by tsunami waves is to simulate the mechanism of wave formation and propagation in order to predict the magnitude of inundation, overtopping, control, design of flood protection structures, and the impact of wave forces in coastal areas [1, 2]. The results obtained from tsunami wave modeling, such as wave run-up height, wave overtopping from the coastline, volume of water crossing the coastline, flow velocity, and water depth, significantly influence the extent of coastal damage. Controlling each of these factors can be a crucial step in reducing the damage.

Tsunami waves act as shallow-water waves due to their long wavelength even in deep waters [3]. The velocity of tsunami waves decreases as they approach shallow coastal waters, depending on the coastal slope, coastal environment, and existing structures. This reduction in velocity, combined with the constant period and reduced wavelength, leads to an increase in wave height due to phenomena such as shoaling and refraction [4, 5]. Due to their long period and long wavelength, tsunami waves are approximated as a single wave [6, 7]. The single wave has a crest that is entirely above the water surface. Water particles in the single wave move forward and become motionless without returning to complete a full cycle. In comparison to oscillatory waves, the single wave has a transitional state and has unlimited wave length and period, thus remaining unchanged in shape and height at a constant depth over time [8, 9].

Numerous laboratory experiments and numerical models have been conducted to simulate solitary wave behavior. Synolakis [10] measured the maximum wave run-up on the shore for 76 waves of specific heights at constant water depth using a two-dimensional simulation of solitary waves in a rectangular channel with a wave maker at one end. Zelt [11] simulated the breaking of solitary waves in a laboratory experiment conducted in a channel, with a water height of 0.21 meters and a wave height-to-water depth ratio of 0.28. They presented a numerical method for calculating water surface elevation and validated the results with experimental data. Honarmand et al. [12] simulated two-dimensional solitary wave generation on a sloping beach using a numerical method without mesh and exponential basis functions. Honarmand et al. [13] simulated the two-dimensional propagation of solitary waves on a sloping beach using the Flow 3D model and validated the results by comparing them with the experimental data from Synolakis [10] for wave run-up and tsunami wave propagation on a steep coast.

Chen et al. [15] investigated the reflection of solitary waves after colliding with a vertical barrier using high-speed cameras and image processing technology. The researchers conducted numerical modeling based on the experimental results, comparing the accuracy of the numerical modeling with existing theoretical methods. The study by Zaqian et al. [16] focused on the flow structure resulting from the propagation of solitary waves on a thin submerged plate. The impact of the submerged plate angle was examined, revealing additional vortices in experiments with a positive angle, while no vortices were observed for a negative angle. Investigation of clockwise vortices behind the submerged plate indicated a decrease in vortex strength with increasing angles in both directions. Wang et al. [17] conducted a study on the interaction between solitary waves and a vertical submerged wave breaker using a numerically developed method based on constrained interpolation profile (CIP), capable of examining the influence of viscosity. After validation, the impact of the submerged wave breaker on the transmission coefficient of solitary waves was assessed. The researchers concluded that the width of the wave breaker has the least effect on the transient characteristics of solitary wave transmission through a submerged structure, while the height of the wave breaker effectively reduces the transmitted wave height. Finally, comparison of output results from semi-analytical relationships with experimental data and real information from the coasts of Vaticano in Italy indicated acceptable results .

Cavaliere et al. [18] presented a semi-analytical relationship for predicting the location of solitary wave breaking on a sloping beach. They conducted an experimental study to propose this relationship. He et al. [19] focused on investigating the influence of bed roughness on the characteristics of solitary wave transmission in their study. They reported that, contrary to the influence of bed roughness on the shape of solitary waves, the peak of the solitary wave is not significantly affected by the roughness. The effect of solitary waves on a submerged floating tunnel was examined by Zou et al. [20]. In this study, the solitary wave amplitude, distance of the submerged tunnel from the wave rising point, cross-sectional geometry of the tunnel, and relative density of two fluids were considered as the study variable parameters. The results showed that using a parametric cross-section for the submerged tunnel instead of circular and elliptical sections can significantly reduce the wave-induced force. A comprehensive investigation was conducted by Huang and Dong [21] utilizing a numerical model to analyze the dynamic interaction between a solitary wave and a submerged dike. The study focused on examining the influence of the solitary wave height and the dimensions of the dike on various factors such as drag force, flow field characteristics above the dike, and wave transformation features. The researchers identified the presence of two distinct vortexes at the right toe and the lee side of the dike, highlighting these locations as potential sites for scour. In a related study, Huang et al. [22] explored the interaction between solitary waves and emergent rigid vegetation. This investigation involved experimental procedures, with the modified Boussinesq equations employed to simulate the laboratory experiments. Key parameters under scrutiny included wave height, vegetation length, and vegetation density. The researchers derived an empirical expression for the mean drag coefficient and observed a notable increase in maximum wave height immediately prior to the vegetation, while also noting a reduction in wave transmission in the presence of dense vegetative cover.

The utilization of the Mike 3D Flow Model FM has become ubiquitous in the realm of hydraulic engineering due to its ability to accurately simulate a wide array of complex hydraulic phenomena. This powerful computational tool has been effectively employed in various studies to address challenges such as scour, sedimentation, flow pattern, and salinity, among others [23, 24, 25, 26]. In addition, numerous research studies in the literature investigated solitary waves and their characteristics. Despite the widespread usage of the MIKE model in study of the hydraulic of coastal structures, less attention was paid to simulate solitary waves by this model. In the present study, the capability of the model for solitary waves simulation is investigated. The validation of the model is done using experimental data presented by Chen et al. [14]. The results of the present study are used to assessment the MIKE model capabilities in the study of the hydraulic of solitary waves and coastal structures.

2. Materials and Methods

2.1. Numerical model

The MIKE 3D Flow Model FM employs the cell-centered finite-volume method and unstructured flexible mesh to discretize the primitive equations in both Cartesian and Sigma-coordinates. This model is based on numerical solutions for the 3D incompressible Reynolds-Averaged Navier–Stokes equations, incorporating the Boussinesq and hydrostatic pressure assumptions. It includes continuity, momentum, heat, salinity, and density equations for comprehensive simulation of fluid flow [27].

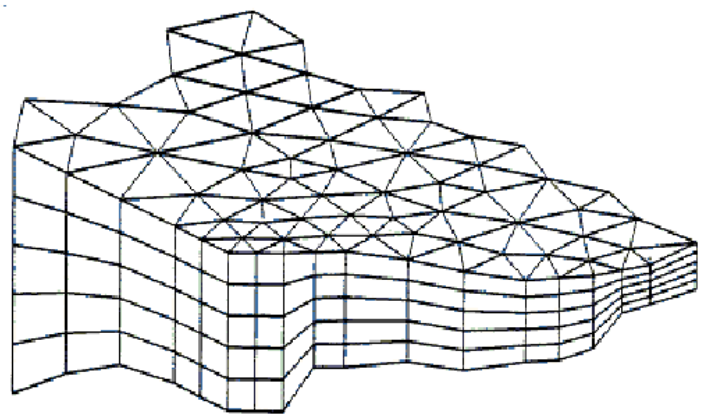

Figure 1. Schematic of unstructured (horizontal direction) and structured (vertical direction) mesh in Mike 3 Flow Model FM [27]

2.2. The governing equations

The continuity and momentum equations in the Cartesian coordinate system are expressed as follows:

The continuity equation is written as:

$$\frac{\partial u}{\partial x}+\frac{\partial v}{\partial y}+\frac{\partial w}{\partial z}=S \tag{1}$$

The momentum equation is written as:

The momentum equation in X direction is written as:

$$\frac{\partial u}{\partial t}+\frac{\partial u^2}{\partial x}+\frac{\partial uv}{\partial y}+\frac{\partial uw}{\partial z}= fv-g\frac{\partial \eta}{\partial x}-\frac{1}{\rho_0}\frac{\partial P_a}{\partial x}-\frac{g}{\rho}\int_z^{\eta}\frac{\partial \rho}{\partial x}dz \tag{2}$$

$$-\frac{1}{\rho_0 h}\left(\frac{\partial s_{xx}}{\partial x}+\frac{\partial s_{xy}}{\partial y}\right)+F_u+\frac{\partial}{\partial z}\left(v_t\frac{\partial u}{\partial z}\right)+u_s S$$

Where t is the time; x, y, and z are the Cartesian coordinates; η is the water surface elevation; d is the still water depth; $h=\eta+d$is the total water depth; u, v, and w are the velocity components in the x, y, and z directions; $f=2\Omega\sin\varphi$ is the Coriolis parameter (Ω is the angular rate of revolution and φ: the geographic latitude); g is the gravitational acceleration; ρ is the water density; S_{xx}, S_{xy}, S_{yx}, and S_{yy} are components of the radiation stress tensor; υ_t is the vertical eddy viscosity; P_a is the atmospheric pressure; and $\rho_0$is the reference density of water. S is the magnitude of the discharge due to point source, u_s and v_s are the velocities of point source in x and y directions, and F_u and F_v are horizontal stress terms.

2.2.1. Turbulence *Models*

Turbulent stress can be modeled based on a concept called eddy viscosity. Eddy viscosity is divided into two types: horizontal eddy viscosity and vertical eddy viscosity. In many numerical modeling approaches, small-scale turbulence cannot be captured by choosing fine spatial discretization. However, this type of turbulence can be accounted for by considering turbulence models.

2.2.2. Vertical eddy viscosity

The viscosity of a vortex is computable based on the logarithmic law (Eq. 3)

.

$$\upsilon_t = U_\tau h\left(c_1\frac{z+d}{h}+c_2\left(\frac{z+d}{h}\right)^2\right) \tag{3}$$

where $U_\tau = max(U_{\tau s}, U_{\tau b})$ and $U_{\tau b}$ and $U_{\tau s}$ are shear of the bed and water surface, as well as the coefficients c_1 and c_2, are 0.41 and -0.41, respectively; h and z represent the water depth and the vertical distance from the bed, respectively.

In the context of the RANS equations for Reynolds stresses, the eddy viscosity plays a crucial role in capturing the turbulent behavior of fluid flow. In the current model, a constant value of 10^{-5} m^2/s has been adopted for the horizontal component of the eddy viscosity. It has been observed that the model's sensitivity to variations in this constant is negligible, indicating a robustness in its predictive capabilities.

2.2.3. Horizontal eddy viscosity

In many cases, the value of horizontal eddy viscosity is considered constant. However, the Smagorinsky relationship expresses turbulence based on characteristic length and deformation ratio, which is a function of flow velocity, as follows:

$$A = c_S^2 l^2 \sqrt{2S_{ij}S_{ij}} \tag{4}$$

$$S_{ij} = \frac{1}{2}\left(\frac{\partial u_i}{\partial x_j}+\frac{\partial u_j}{\partial x_i}\right) \tag{5}$$

Where, c_s is the constant Smagorinsky coefficient; l is a characteristic length; S_{ij} is a deformation ratio and A is a horizontal eddy viscosity value.

2.3. Evaluation of the Numerical Model

Solving the theory of solitary waves

The water surface elevation in solitary waves is determined by solving analytical equations 6 and 7, While the flow velocity is calculated using equation 8 [28, 29].

$$SE(t) = H\sec h^2\left[\left(\frac{3H}{4h}\right)^{1/2}\frac{C}{h}(t-t_{\max})\right] \tag{6}$$

$$C = [g(H+h)]^{1/2} \tag{7}$$

$$u(t) = C\frac{SE(t)}{SE(t)+h} \tag{8}$$

Where, $SE(t)$ is a water surface level, h represents the water level, H denotes the wave height, c stands for the solitary wave velocity, t represents time, t_{max}signifies the wave crest occurrence time, g represents the acceleration due to gravity, and $u(t)$ denotes the water current velocity.

2.4. Numerical Simulation Components

The solution domain on the plane (Figure 2) is discretized using flexible rectangular structured meshes with dimensions of 1 square centimeter per element and 15 uniform vertical layers of the sigma type. In optimizing the mesh dimensions for our study, careful consideration was given to ensure independence from grid sizes and minimize computational time. To achieve this, a series of tests were conducted using both small and large mesh sizes, with the resulting wave velocity fluctuations meticulously recorded. Ultimately, the mesh size yielding the minimum velocity fluctuations was selected for our analysis. In the simulation, the effect of shear stress between water and walls due to the smoothness of the walls, as well as the effect of shear stress between water and air, were not considered. Additionally, in order to ensure numerical stability and accuracy in the results, a Courant number of 1 was chosen, and the simulation was executed with a time step of 0.05 second.

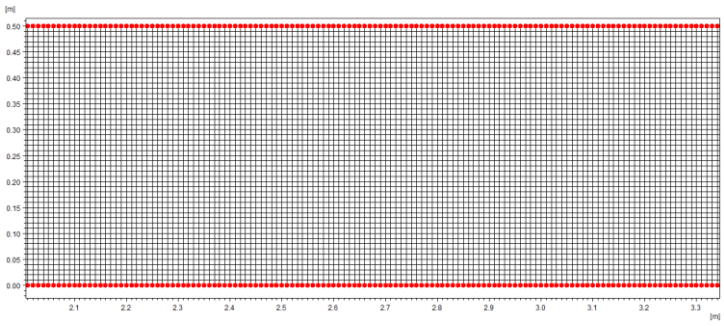

Figure 2. A plan view of computational domain mesh

In this study, the potential of the MIKE 3 Flow Model FM in simulating tsunami waves was evaluated using experimental data provided by the Hydraulic Engineering Department of Changsha University in China by Chen et al. [14]. Figure (3) illustrates a cross-section of the experimental model. The canal has 40 meters long, 0.5 m wide, and 0.8 m high. At the beginning of the canal, a tsunami wave is generated using a piston, while at the channel end, a sedimentary beach with a length of 7.5 m is located. The beach has a variable slope ranging from 1:10 over a length of 3.5 m to 1:20 over a length of 4 meters towards the beginning of the canal. Natural sediment particles with an average diameter of 0.368 mm were used as the beach sediment bed in the experimental model. The generated wave height was 0.15 m, and the initial water depth was 0.35 m. For wave surface elevation, water level changes, and flow velocity measurements, 7 wave gauges (Canadian RBR Limited Liability Company model), 4 ultrasonic water level gauges (Beijing Sinfotek Science and Technology Co., Ltd), and 3D acoustic Doppler velocity sensors (Norway Nortek AS) were utilized. Additionally, a Logitech C910 HD Webcam with a resolution of 1MP was used to capture momentary images of the advancing and receding wave flow alongside the flume. The positioning of the gauges is as shown in Figure (3).

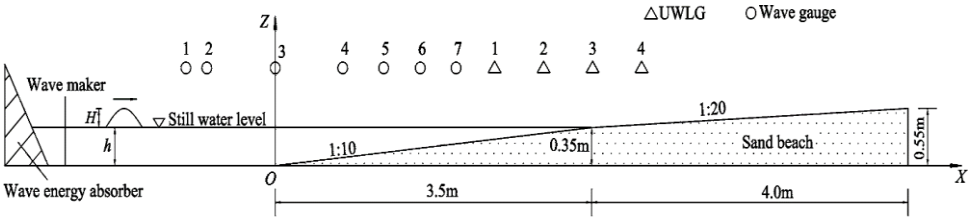

Figure 3. Cross-sectional view of experimental set-up [14].

In order to discern the disparities in values between the outcomes derived from simulation and analytical relationships and experimental data, various evaluation indicators such as Mean Absolute Deviation (MAD), Mean Squared Error (MSE), Root Mean Squared Error (RMSE), and Coefficient of Determination (CD) R^2 were employed. When considering the first three indices, values approaching zero signify an enhancement in the accuracy of the modeling outcomes. Furthermore, a coefficient of determination nearing 1 indicates a favorable correspondence between analytical and modeling results. It is possible to quantify the four performance assessment parameters used in this research using Equations (9) to (12).

$$\mathrm{MAD}=\frac{1}{N}\sum_{i=1}^{N}(p_i-\bar{p}) \tag{9}$$

$$\mathrm{MSE}=\frac{1}{N}\sum_{i=1}^{N}(P_i-O_i)^2 \tag{10}$$

$$\mathrm{RMSE}=\sqrt{\frac{1}{N}\sum_{i=1}^{N}(P_i-O_i)^2} \tag{11}$$

$$\mathrm{CC}=\frac{\sum_{i=1}^{N}(P_i-\bar{P})(O_i-\bar{O})}{\sqrt{\sum_{i=1}^{N}(P_i-\bar{P})^2\sum_{i=1}^{N}(O_i-\bar{O})^2}} \qquad -1\le CC\le 1 \tag{12}$$

where O_i and P_i are, respectively, the observed and the predicted values, $\bar{O}$ is the average of observed values and N is the quantity of observations.

3. Results and Discussion

3.1. Numerical Model Validation

In the initial phase, a comparison was conducted between the outcomes derived from the existing analytical calculations (Eqs. 6-8) and the results obtained from numerical simulations, with the aim of validating and confirming the software. The water depth utilized in these calculations and simulations was standardized at 35 cm, while the ratio of wave height to water depth was simulated at 0.28, 0.42, and 0.57. In order to ensure the numerical software's precision and dependability, several models were assessed to determine adjustable coefficients within the software. This was done to align the simulation results as closely as possible with the analytical values. After several rounds of trial and error, specific values were assigned to the Smagorinsky coefficient (c_S), maximum vertical eddy viscosity, and bed roughness height, as detailed in Table (1). This was carried out to minimize discrepancies between the modeling results and the analytical findings.

The simulation results pertaining to wave velocity and wave surface elevation, as well as their comparison with the output of analytical equations (equations 6 to 8), are depicted in Figure 4. Upon examination of the results presented in this figure, it is evident that while the flow velocity (u) and wave surface elevation (SE) obtained from the software demonstrate a reasonable level of agreement with the results derived from analytical equations, the accuracy of the modeling results diminishes somewhat in comparison to the analytical results as the wave height to water depth ratio (H/h) increases.

Table 1. Calibration of the Numerical Model Coefficients

Parameter	Value	Dimension
Smagorinsky coefficient (c_S)	0.18	-
Maximum vertical eddy viscosity	0.4	**m^2/s**
Manning coefficient (n)	0.01	-

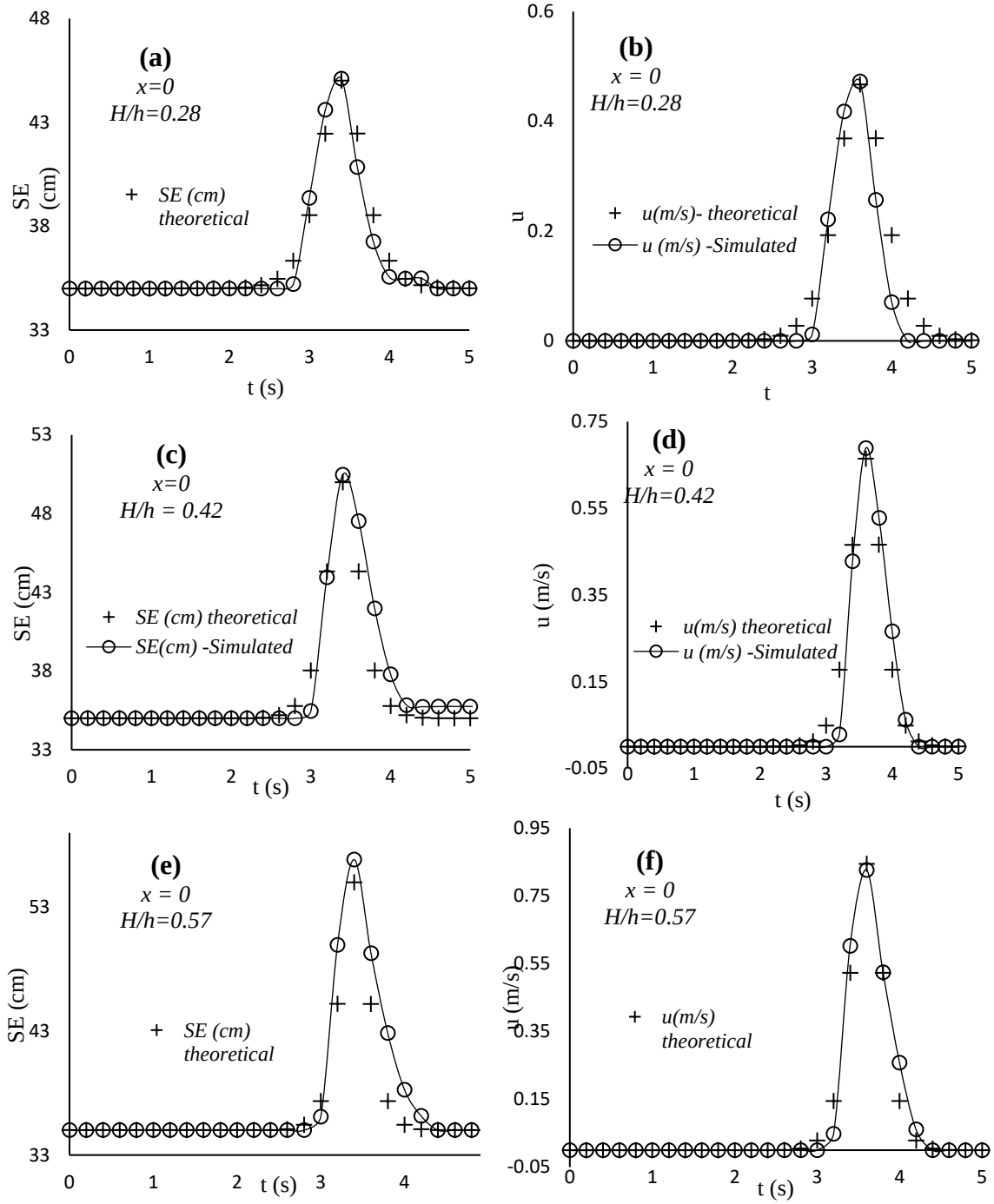

Figure 4. (b, d, f): a comparison of wave velocity (*u)* and (a, c, e): wave surface elevation (*SE*) obtained from numerical simulation and analytical solutions

A comparative analysis of the results derived from analytical relationships and modeling using the aforementioned evaluation indices is delineated in Table (2). Upon scrutiny of the indices for two parameters, wave velocity and wave surface elevation, it is apparent that while the software generally yields satisfactory results in solitary wave modeling, the accuracy of modeling outcomes diminishes with an escalation in the ratio of wave height to water depth (*H/h*). Additionally, based on the findings presented in Table (2), the software demonstrates relatively greater proficiency in computing wave velocity as opposed to modeling wave surface elevation, given that the errors accrued in the wave surface elevation segment are more pronounced for a constant *H/h* ratio. It is imperative to note that the term "n" in Table (2) pertains to the quantity of data points utilized for result comparison.

Table 2. The output indicators of evaluation for comparing the results of simulation and analytical relationship results.

-	**H/h= 0.57 u(m/s)**	**H/h= 0.57 SE (cm)**	**H/h= 0.42 u (m/s)**	**H/h= 0.42 SE (cm)**	**H/h= 0.28 u(m/s)**	**H/h= 0.28 SE (cm)**
n	31	31	31	31	31	**31**
MAD	0.048	1.15	0.033	0.78	0.017	**0.25**
MSE	0.015	10.84	0.006	2.88	0.0013	**0.27**
RMSE	0.124	3.29	0.077	1.69	0.037	**0.52**
R^2	0.79	0.78	0.89	0.90	0.95	**0.97**

3.2. Investigating the potential of numerical model in wave simulation

The study delves into the potential of numerical modeling in simulating wave behavior, with a particular focus on its application in assessing tsunami waves. The accuracy and limitations of the numerical model are rigorously evaluated through statistical analysis and comparison with experimental data. Upon validation of the numerical model using established wave theory equations, the investigation progresses to the examination of its capability in replicating tsunami waves based on experimental results. The findings, analyzed using specified evaluation indicators, reveal a strong concordance between the model's output and the actual data, particularly at specific positions along the simulated channel.

Notably, the highest degree of modeling accuracy is observed at certain positions, such as x = 3.5 m for water surface elevation estimation and x = 0.5 m for flow velocity estimation. These findings are supported by the lowest root mean square error (RMSE) and the highest coefficient of determination (R^2). However, it is crucial to acknowledge that the utilized numerical model, the Mike 3 Flow Model FM, rendering it incapable of accurately simulating severe water surface elevation and flow velocity oscillations. The comparison between the numerical results and experimental data highlights minor discrepancies, particularly evident in the inability of the model to precisely replicate extreme water surface elevation and flow velocity oscillations, as depicted in Figures 5 (d) and (f). The examination extends to the analysis of water surface elevation and flow velocity at various sections along the channel length. The results demonstrate a discernible reduction in water surface elevation as the wave encounters the shoreline slope, followed by a substantial decrease upon crossing the shoreline. Specifically, there is a gradual decrease in wave crest height from 15 cm to 10.5 cm over a 3.5 m initial slope length, and a further reduction from 10.5 to 7.5 cm over a 0.5 m distance after the shoreline (Figs 5 a, b, c).

Conversely, the water flow velocity exhibits an increase as it traverses the shoreline slope, from 0.8 to 1.4 m/s (Fig. 5 e). Furthermore, the presence of negative velocity values indicates instances of wave flow reversal at specific positions along the channel, signifying complex wave dynamics (Figs. 5 e, f, g, h).

Table 3. A comparative analysis of numerical model results and experimental data utilizing statistical characteristics

	u (m/s)				***SE* (cm)**			
-	x=2.5 m	x=2.2 m	x=1.5 m	x=0.5 m	x=4m	x=3.5m	x=2.5m	**x=0**
n	51	51	51	51	51	51	51	**51**
MAD	0.09	0.05	0.08	0.04	0.98	0.29	0.94	**0.25**
MSE	0.02	0.01	0.02	0.00	1.96	0.24	5.26	**0.27**
RMSE	0.13	0.11	0.14	0.07	1.40	0.49	2.29	**0.52**
R^2	0.93	0.91	0.77	0.92	0.97	0.99	0.75	**0.97**

In the context of flow rate per unit width, the value at position x=0 decreases from 0.55 m^3/s-m due to the slope of the shore. At distances x=3.5 m and x=7 m, the value further decreases to 0.14 m3/s-m and 0.02 m3/s-m, respectively. The flow experiences a reversal at distance x=0 starting at 2.5 seconds and continues until the end of the simulation, with a maximum value of 0.04 m^3/s-m (Figure 6). The maximum flow velocity varies with wave position, as illustrated in Figure (7a) it reaches 0.72 m/s in the middle part of the wave crest, 1.3 m/s at the shore slope position (Figure 7b), and 2.1 m/s when crossing the shoreline (Figure 7c). A backflow velocity of 0.96 m/s is observed at the shoreline (Figures 7d and e).

Figure 8 provides a visualization of the vectors and streamlines of water velocity for the central section of the flow at the 7th second of simulation. The vectors depict the path of water flow in different depth layers, indicating the wave flow reversal at the 7th second along the shoreline (at a distance of x=3.5 m). However, it is noteworthy that the maximum flow velocity according to the numerical results is 2.1 m/s, occurring at a distance of 30 cm from the shoreline (Fig. 7c). The observed increase in flow velocity can be attributed to the decrease in water surface elevation at the shoreline.

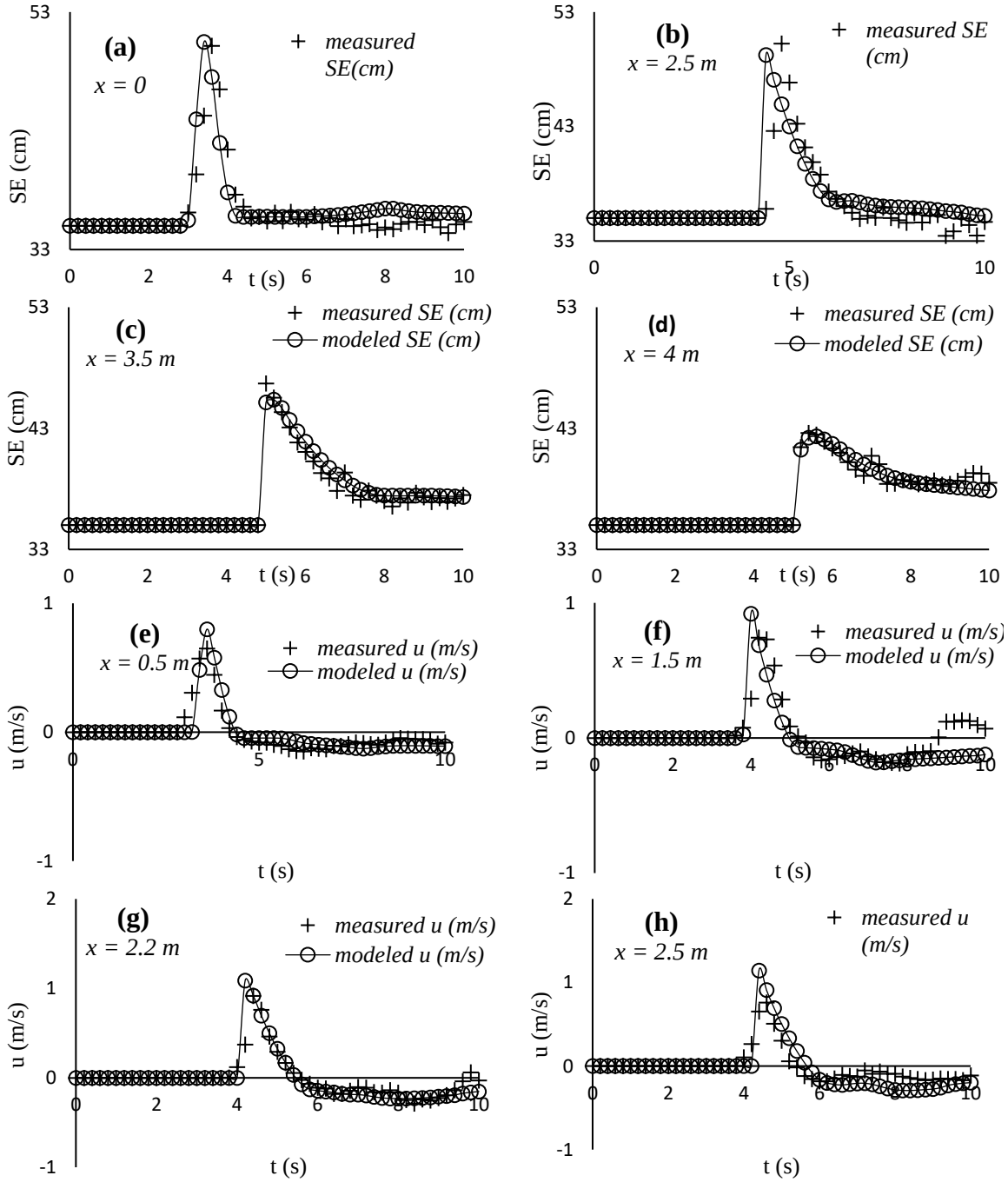

Figure 5. A comparison of wave velocity (u) and wave surface elevation (se) obtained from numerical modeling and experimental results

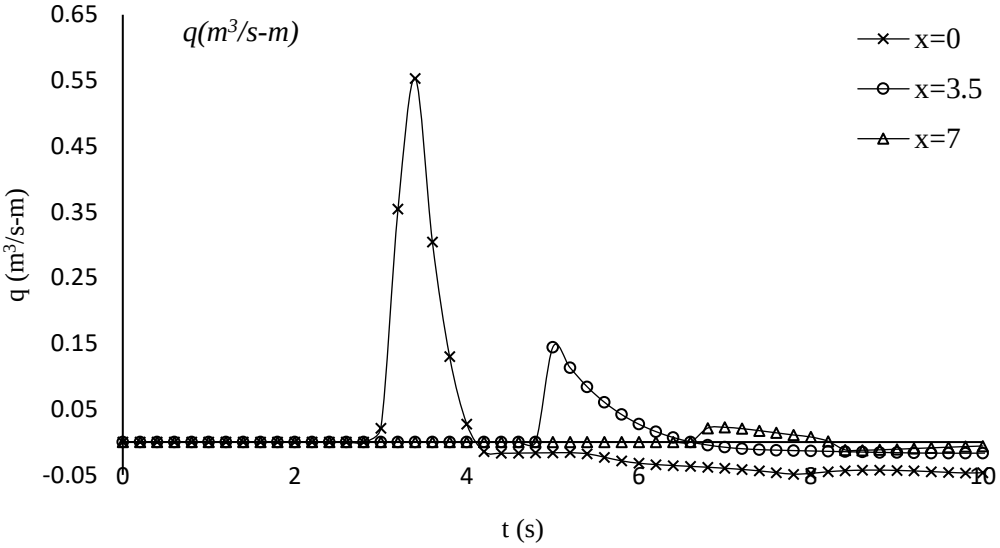

Figure 6. Flow rate per unit width at x=0, x=3.5 m and x=7 m

(a)

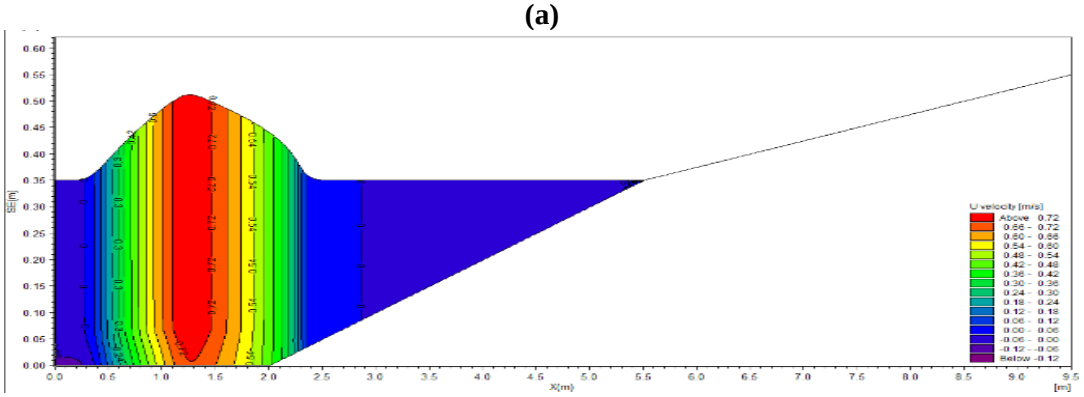

(b)

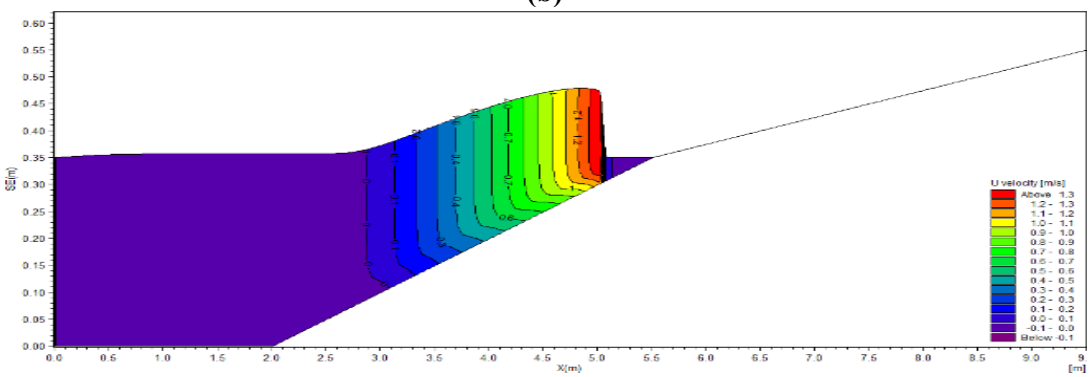

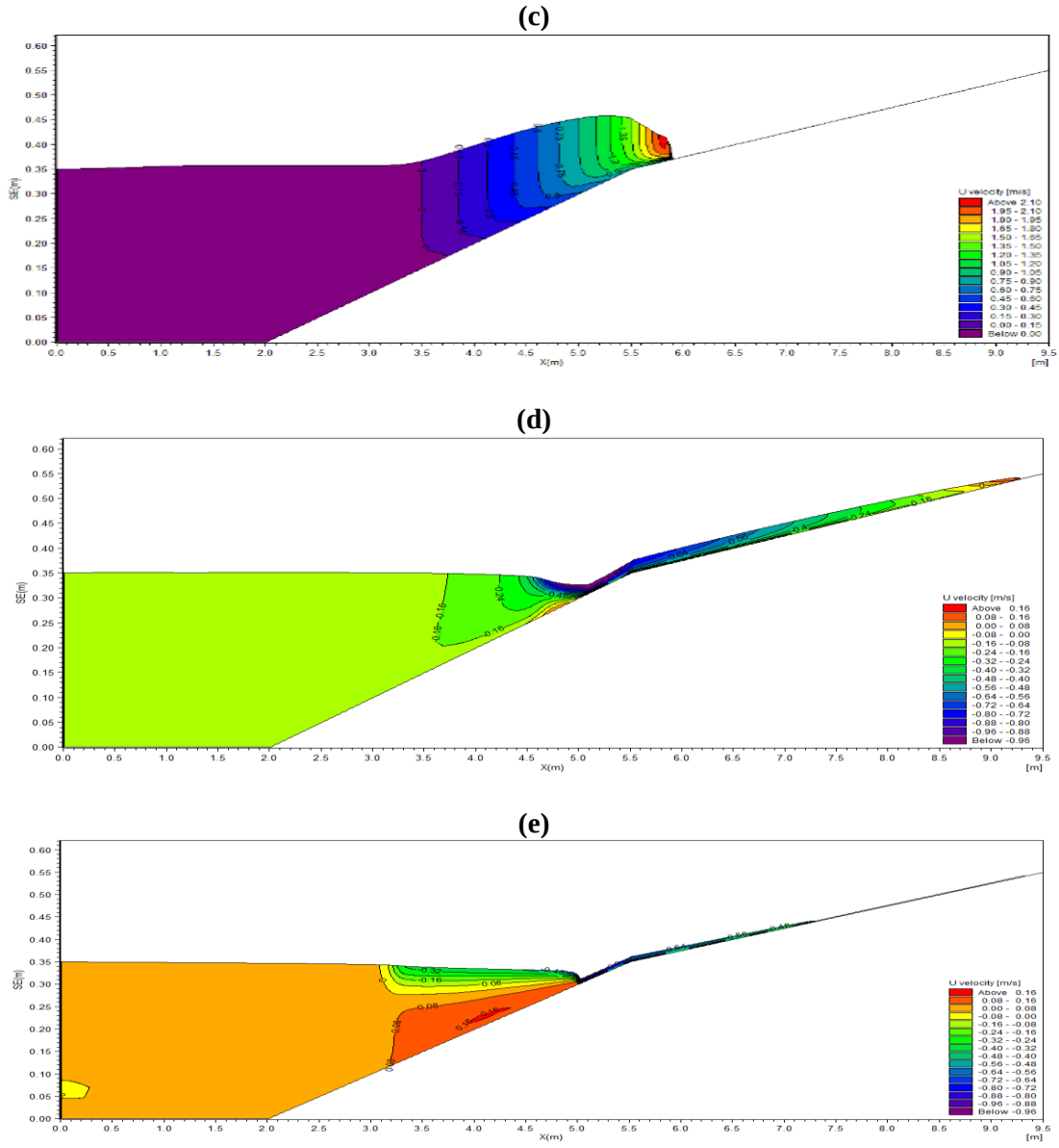

Figure 7. Profile of flow velocity and water surface elevation; a) before the wave reaches the shore slope, b) inside the shoreline, c) Crossing the coastline, d) Rising wave on the beach, e) returned wave (In the longitudinal axis, positive values represent velocity in the forward direction, while negative values represent velocity in the opposite direction).

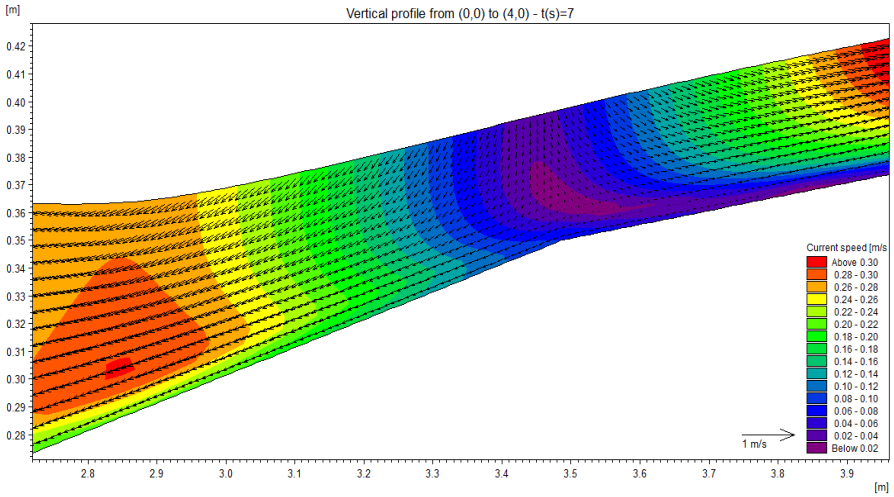

Figure 8. Profile of flow velocity and velocity vectors in 7th seconds of simulation

4 Conclusion

In the current investigation, the study focused on evaluating the ability of the Mike 3 Flow Model FM in accurately simulating free-surface flows, particularly tsunami waves. The numerical model underwent calibration and validation using experimental data conducted by Chen et al. [14] at Changsha University, China, in 2015. Evaluation indices including Mean Absolute Deviation (MAD), Mean Squared Error (MSE), Root Mean Squared Error (RMSE), and Coefficient of Determination (R^2) were utilized to assess the variance between the simulation results and the experimental data.

While minor disparities were noted at certain points between the simulation results and the experimental data, the comparison distinctly demonstrates that the three-dimensional model adeptly captures the dynamics of non-steady flows throughout the entire observation period. Furthermore, the three-dimensional model has the capability to furnish comprehensive and precise insights into the physical parameters of wave evolution in both spatial and temporal dimensions, encompassing water depth, wave height characteristics, flow velocity, wave front propagation distance, and other pertinent factors.

Upon comparing the numerical results with experimental data, it became evident that the accuracy of the numerical model in simulating wave velocity (RMSE $\leq$ 0.14) surpassed its performance in simulating wave surface elevation (RMSE $\leq$ 2.29). This disparity underscores the nuanced nature of wave dynamics and highlights the need for continued refinement in numerical modeling approaches. Overall, these findings underscore the potential of the numerical model in capturing wave dynamics, particularly in scenarios where the ratio of wave height to water depth is low. However, further research and validation against diverse experimental datasets are warranted to fully ascertain the robustness and generalizability of the numerical package. In light of the current investigation, it is imperative to recognize that our focus has been primarily on analyzing the flow pattern. However, it is essential to emphasize the necessity for additional research to assess the efficacy of the aforementioned numerical model in simulating erosion and sedimentation patterns. This further exploration will provide a more comprehensive understanding of the model's capabilities and limitations in replicating real-world scenarios. Consequently, such research will contribute to the advancement of knowledge in this field and facilitate the development of more accurate and reliable numerical models for practical applications.

5 References

1. Camfield, F.E., 1980. Tsunami Engineering. Special Report No. 6. US Army Corps of Engineers, CERC, Ft. Belvoir, VA.
2. Xie, J., (2007). Numerical modeling of tsunami waves (Doctoral dissertation, University of Ottawa (Canada)).
3. Bandyopadhyay, A., Manna, S. and Maji, D., (2021). Hydrodynamic aspects of tsunami wave motion: a review. Ocean Dynamics, 71(5), pp.613-629.
4. Harbitz, C.B., Løvholt, F., Pedersen, G. and Masson, D.G., (2006). Mechanisms of tsunami generation by submarine landslides: a short review. Norwegian Journal of Geology/Norsk Geologisk Forening, 86(3).
5. Yavari-Ramshe, S. and Ataie-Ashtiani, B., (2016). Numerical modeling of subaerial and submarine landslide-generated tsunami waves—recent advances and future challenges. Landslides, 13, pp.1325-1368.
6. Madsen PA, Fuhrman DR, Schaeffer HA (2008) On the solitary wave paradigm for tsunamis. J Geophys Res. doi:10.1029/2008jc004932.
7. Costa, P.J. and Andrade, C., (2020). Tsunami deposits: present knowledge and future challenges. Sedimentology, 67(3), pp.1189-1206.
8. Hammack, J.L. and Segur, H., (1974). The Korteweg-de Vries equation and water waves. Part 2. Comparison with experiments. Journal of Fluid mechanics, 65(2), pp.289-314.
9. Oetjen, J., Sundar, V., Venkatachalam, S., Reicherter, K., Engel, M., Schüttrumpf, H. and Sannasiraj, S.A., (2022). A comprehensive review on structural tsunami countermeasures. Natural Hazards, 113(3), pp.1419-1449.
10. Synolakis, C.E., (1987). The runup of solitary waves. Journal of Fluid Mechanics, 185, pp.523-545.
11. Zelt, J. (1991). "The run-up of nonbreaking and breaking solitary waves." Coastal Engineering **15**(3): 205-246.
12. Honarmand M, Shanehsazzadeh A, Zandi M, Vahida A. Numerical Simulation and Experimental Study on Tsunami Propagation and Run-up and the Influence of Submerged Breakwater on Run-up. Journal of Oceanography 2019; 9 (36) :31-38. URL: http://joc.inio.ac.ir/article-1-1248-fa.html.
13. Honarmand M , Zandi M, Shanehsazzadeh A., (2016). 2D Numerical simulation of solitary waves propagation nearly beach in order to determination of tsunami waves run-up. Civil engineering conference 2016. Ferdowsi university of Mashhad, Mashhad, Iran.
14. Chen, J., Huang, Z., Jiang, C., Deng, B. and Long, Y., (2012). An experimental study of changes of beach profile and mean grain size caused by tsunami-like waves. Journal of Coastal Research, 28(5), pp.1303-1312.
15. Chen, Y.Y., Kharif, C., Yang, J.H., Hsu, H.C., Touboul, J. and Chambarel, J., (2015). An experimental study of steep solitary wave reflection at a vertical wall. European Journal of Mechanics-B/Fluids, 49, pp.20-28.
16. Zaqian, R., et al. (2017). Experimental study of flow structures of a solitary wave propagating over a submerged thin plate in different angles using PIV technique. International Journal of Heat and Fluid Flow 66: 18-26.
17. Wang, J., et al. (2018). Numerical study on interaction of a solitary wave with the submerged obstacle. Ocean engineering 158: 1-14.
18. Cavaliere, D., la Forgia, G., Adduce, C., Alpers, W., Martorelli, E. and Falcini, F. (2021). Breaking location of internal solitary waves over a sloping seabed. Journal of Geophysical Research: Oceans 126(2): e2020JC016669.

19. He, J.H., Qie, N. and He, C.H., (2021). Solitary waves travelling along an unsmooth boundary. Results in Physics, 24, p.104104.
20. Zou, P.X., Bricker, J.D. and Uijttewaal, W.S., (2021). The impacts of internal solitary waves on a submerged floating tunnel. Ocean Engineering, 238, p.109762.
21. Huang, C. J., & Dong, C. M. (2001). On the interaction of a solitary wave and a submerged dike. Coastal Engineering, 43(3-4), 265-286.
22. Huang, Z., Yao, Y., Sim, S. Y., & Yao, Y. (2011). Interaction of solitary waves with emergent, rigid vegetation. Ocean Engineering, 38(10), 1080-1088.
23. Soudi, Mina, Hojjat Ahmadi, Mehdi Yasi, Stefano Sibilla, Andrea Fenocchi, and Sajad Ahmad Hamidi (2019). Investigation over the capability of MIKE 3 flow model FM to simulate the hydrodynamics and salinity distribution of hypersaline lakes: Lake Urmia (Iran) as case study." Coastal Engineering Journal 61, no. 4. 486-501.
24. Hemmati, Mohammad, Hojjat Ahmadi, Sajad Ahmad Hamidi, and Vahid Naderkhanloo. (2021). "Environmental effects of the causeway on water and salinity balance in Lake Urmia." Regional Studies in Marine Science 44. 101756.
25. Bigdeli-Tabar-Sahreini, H., Hemmati, M., Ahmadi, H., Naderkhanloo, V. (2018). 'Numerical Investigation of the Effect of Groins and Bendway Weirs on Flow and Sediment Pattern Using Mike 3 Flow Model FM', Water and Soil Science, 28(1), pp. 159-171.
26. Naderkhanloo, V., Soudi, M., Hemmati, M. and Hamidi, S.A., 2017. 3D Numerical simulation of dam-break flows with sediment transport over movable beds. In World Environmental and Water Resources Congress 2017 (pp. 161-170).
27. MIKE 3 User Guide and Reference Manual, Danish Hydraulic Institute (DHI) (2007). Water and Environment, Denmark.
28. Goring, D.G., (1979). Tsunamis-The propagation of long waves on to a shelf. California Institute of Technology, Pasadena.
29. Li, Y., and F. Raichlen (2003), Energy balance model for breaking solitary wave run-up, J. Waterway, Port, Coast Ocean Eng., 47, 47–59.